Journal of Materials Science: Materials in Electronics (2019) 30:609–623
https://doi.org/10.1007/s10854-018-0327-z

The effect of Yb^{3+} ion substitution on dielectric and microstructural properties of $Y_3Al_5O_{12}$ ceramics

M. A. Almessiere[1,3] · B. Unal[2] · A. Baykal[3] · I. Ercan[4]

Received: 5 September 2018 / Accepted: 31 October 2018 / Published online: 2 November 2018

Abstract
The electrical and dielectric properties of $Y_3Al_5O_{12}$ (yttrium aluminum garnet, YAG) ceramics are investigated in detail. YAG:(Yb)x ($0.01 \le x \le 0.09$) was synthesized by a solid state reaction and characterized by X-ray powder diffraction, field emission scanning electron microscopy, and high-resolution transmission electron microscopy. The electrical and dielectric properties have been intensively studied under certain bias voltages up to a frequency of 10 MHz. These properties are dependent on the substitution rates, independent of the bias voltages. The experimental result shows that Yb^{3+} ion substitution into YAG ceramics significantly influences the conductivity, dielectric constant, and lossy mechanisms, which is probably owing to the 3d-Al ions and 4f-Yb ions incorporated at different positions of structural symmetries in $Y_{3-x}Yb_xAl_5O_{12}$ ($0.00 \le x \le 0.09$) ceramics.

1 Introduction

$Y_3Al_5O_{12}$ (YAG) ceramics are considered as a promising material for microwave dielectric ceramics used as substrate materials in microwave electronic devices, such as filters, duplexers, resonators, and other components [1–5]. Substrate applications require additional properties, such as a low temperature coefficient of resonant frequency τ_f, low linear coefficient of thermal expansion, high quality factor (Q×f) values, and high thermal conductivity [4, 6]. High and moderate permittivity ($\varepsilon_r > 20$) materials are used for microwave resonator applications to reduce the size of circuits and devices [2]. Whereas, low permittivity ($\varepsilon_r < 15$) materials are mostly used for substrate applications [2, 7]. Ceramics with a low permittivity can increase the speed of signal propagation through the substrate and reduce the cross-coupling effect with conductors [6]. To modify the dielectric properties of a material, doping with small ratios are predominantly used [8–10]. Substitution with ions from different valence and radii or increased concentration of oxygen voids can generate various physical properties [11–13]. Therefore, doped YAG with trivalent rare-earth ions as a substitution of either Y^{3+} or Al^{3+} sites without changes to the cubic structure is expansively used to obtain a high dielectric performance and low dissipation factor of the capacitors [14]. YAG crystals are complex oxides with the chemical formula $A_3B_2C_3O_{12}$ and belong to the Ia–3a space group, where A, B, and C are cations commonly from metals with various sizes, and B and C can be added from the same element. (A) Cations occupy the dodecahedral site, (B) cations occupy the octahedral site, and (C) cations occupy the tetrahedral site and connect with oxygen ions to form the garnet crystal [15]. The large ion Y^{3+} mainly occupies the (A) site, while Al^{3+} dominates (B) sites [16]. In this study, the microstructure and dielectric properties of Yb^{3+}-substituted YAG ($Y_{3-x}Yb_xAl_5O_{12}$ ($0.00 \le x \le 0.09$)) ceramics were investigated in detail.

✉ M. A. Almessiere
malmessiere@iau.edu.sa

[1] Department of Physics, College of Science, Imam Abdulrahman Bin Faisal University, P.O. Box 1982, Dammam 31441, Saudi Arabia

[2] Departments of Software and Computer Engineering, Istanbul Sabahattin Zaim University, Halkali Cad. No: 2, 34303 Kucukcekmece, Istanbul, Turkey

[3] Department of Nano Medicine Research, Institute for Research & Medical Consultations (IRMC), Imam Abdulrahman Bin Faisal University, P.O. Box 1982, Dammam 31441, Saudi Arabia

[4] Biophysics Department, Institute for Research & Medical Consultations (IRMC), Imam Abdulrahman Bin Faisal University, P.O. Box 1982, Dammam 31441, Saudi Arabia

2 Experimental procedure

The $Y_{3-x}Yb_xAl_5O_{12}$ ($0.00 \le x \le 0.09$) ceramics were synthesized by a solid-state reaction method. Y_2O_3 (99.9%, US-Nano) and Al_2O_3 (99.9%, US-Nano) were used as the initial materials for the preparation of $Y_3Al_5O_{12}$ (YAG) with a chemical ratio of 3:5. For the typical synthesis of $Y_{3-x}Yb_xAl_5O_{12}$ ($0.00 \le x \le 0.09$) ceramics, the stoichiometric amount of Yb_2O_3 (99.9%, US-Nano) was added to the YAG. The starting materials were mixed and ground by an agate mortar and pestle for between 30 min to 1 h to ensure a homogeneous mixture was obtained and to bring fresh surfaces into contact, in order to speed up the reaction process. Each sample was subjected to the same process separately. The mixture was pelletized using a hydraulic press machine under a pressure of approximately 60 kg/m^2 for 80 s. Pelletizing helps to increase the contact area between grains. After grinding and pelletizing, the mixture was prepared for the heat treatment process, and the pellets were placed in a closed alumina crucible. The crucible was closed using a lid to prevent contamination; the pressure caused by the lid may be another factor that guarantees the completion of the reaction. The heating process was carried out in three stages; in each heating step the pellets were ground and pelletized again. Firstly, the samples were subject to a sintering temperature of about 1300 °C for 12 h. Then, the samples were ground and peptized to prepare them for the second stage at 1500 °C for 4 h. The final stage was carried out at about 1600 °C for 2 h. The phase identification of products was conducted by X-ray powder diffraction using a Shimadzu XRD 6100 X-ray diffractometer (Cu K_α radiation, $\lambda = 1.540$ Å). The diffraction data were collected over the 2θ range of 20°–70° with a scanning step width of 0.02°. The morphology, microstructure, and chemical analysis were taken via a FEI Titan S/TEM microscope operating up to 300 kV coupled with an EDXS Si(Li) detector. The dielectric measurements were carried out using Novocontrol Technologies, Alpha-AN with a frequency range of 3 μHz–20 MHz.

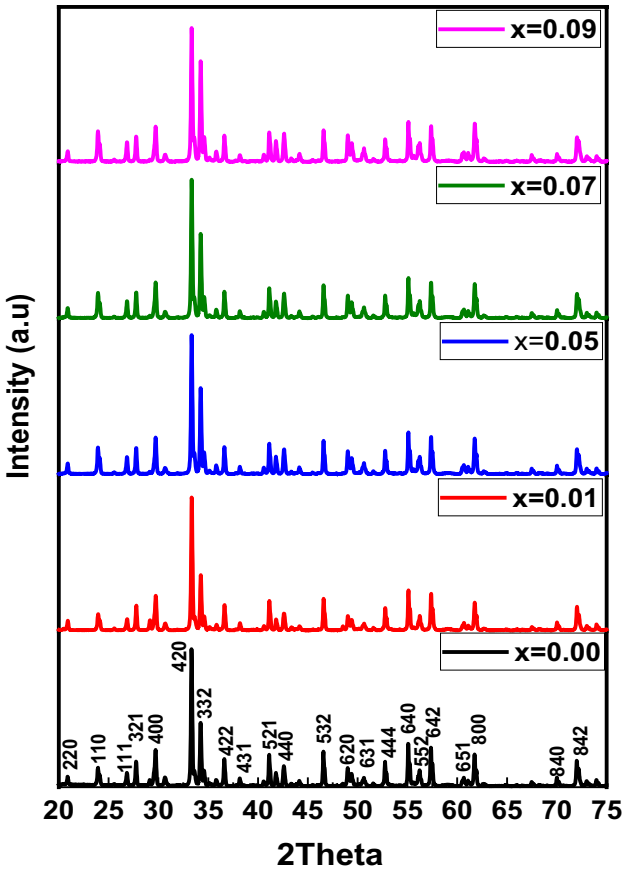

Fig. 1 XRD pattern of YAG: xYb^{3+} with different concentration of Yb^{3+} ions

Table 1 The lattice parameters of $Y_{3-x}Yb_xAl_5O_{12}$ ($0.00 \le x \le 0.09$) ceramics

x	a = b = c (Å)	V (Å)^3
0.00	12.0044	1729.9016
0.01	12.0041	1729.7719
0.05	12.023	1729.3826
0.07	12.0011	1728.4751
0.09	12.0004	1728.17227

3 Results and discussion

3.1 Structural analysis

The XRD powder patterns of the $Y_{3-x}Yb_xAl_5O_{12}$ ($0.00 \le x \le 0.09$) ceramics are presented in Fig. 1. The XRD peaks show a well-crystalline YAG phase with little appearance of the secondary phase of $YAlO_3$ (YAP) according to the database in Match3! with card no. [96-153-3070]. In addition, the crystallographic structure of $Y_{3-x}Yb_xAl_5O_{12}$ ($0.00 \le x \le 0.09$) ceramics were confirmed by Riveted refinement using Match3! Software. A cubic structure was confirmed for the YAG:Yb^{3+} phosphor with different concentrations, as shown in Table 1. We detected a slight decrease in the lattice parameters when increasing the Yb^{3+} concentration, as shown in Fig. 2. This change is principally attributed to the substitution of Y^{3+} ions with an ionic radius of 0.90 Å by ions of Yb^{3+} with a smaller ionic radius of 0.86 Å. Moreover, changing the concentrations of the doped Yb^{3+} ions in the YAG lattice releases stress

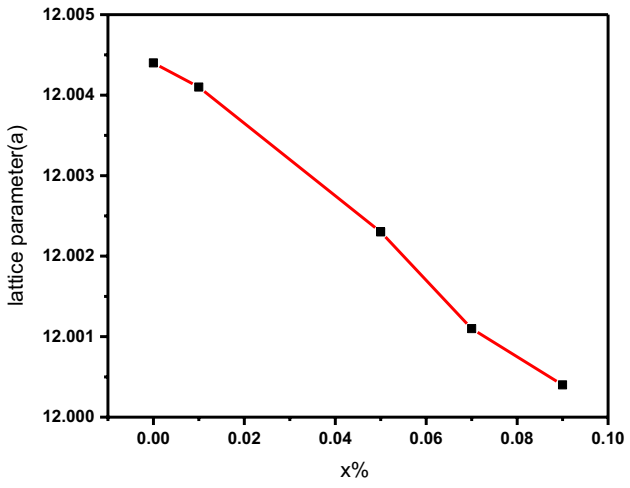

Fig. 2 Relationship between the lattice parameters and concentration of Yb^{3+}

between the perovskite units, resulting in a decrease in the lattice parameters [17, 18].

3.2 Morphological and microstructural analyses

The morphology of the $Y_{3-x}Yb_xAl_5O_{12}$ $(0.00 \le x \le 0.09)$ ceramics are presented in Fig. 2. The images reveal a semi-spherical shape with a homogeneous microstructure. The particles tended to form irregular aggregates and clusters with well-defined grain boundaries. Moreover, the particle sizes decreased slightly with the increasing content of Yb^{3+}, this confirmed the XRD results that the substitution shrunk the crystal. Figure 3 exhibits the TEM images of $Y_{3-x}Yb_xAl_5O_{12}$ for $x = 0.00$, 0.05, and 0.09. They show irregular morphologies with sharp edges and are characterized by a cubic garnet-like structure. HR-TEM images were obtained for measuring the lattice d-spacings, as shown in Fig. 4. The d-spacings show values of 0.21, 0.26, 0.30, 0.32, and 0.42 nm that correspond to the (440), (420), (400), (321), and (220) atomic planes, respectively, that approved the YAG cubic structure. The EDX elemental mapping spectra and quantitative analysis confirmed the formation of the $Y_{3-x}Yb_xAl_5O_{12}$ ceramics for $x = 0.00$ and 0.05, as displayed in Fig. 5.

3.3 Electrical conductivity and dielectric properties

3.3.1 Conductivity

The conductivity under the external electric field exhibits some typical ohmic properties, possibly caused by identical carriers at different DC bias potentials. The overall electrical conductivity can be defined by the equation $\sigma = \sigma_{DC} + \sigma_{AC}$ (where σ_{DC} is the DC conductivity that is usually attributed to the drift of the charge carriers in the electrode and grain interface; σ_{AC} is the AC conductivity related to a dielectric relaxation of the bound charge carriers under a stimulus of the AC electric field). Thus, the DC conductivity is suppressed at low frequencies, whereas AC conductivity is more effective at higher frequencies.

The conductivity of the $Y_{3-x}Yb_xAl_5O_{12}$ $(0.00 \le x \le 0.09)$ ceramics was measured at room temperature in the bias voltage range of − 10.0 to 10.0 V ($\Delta V = 1.0$ V) as a function of the frequency up to 10.0 MHz. In Fig. 6, the frequency dependence of the conductivity for YAG:$x$$Yb^{3+}$ ceramics is calculated from a standard equation [19]:

$$\sigma'(\omega;V) = \sigma_{AC}(\omega;V) = \varepsilon''(\omega;V)\omega\varepsilon_0$$

where $\sigma'(\omega;V)$ is the real component of the complex conductivity, ε'' is the imaginary part of the complex dielectric permittivity (ε^*), ε_0 is the vacuum permittivity, and ω is the angular frequency of the AC stimulation signal applied across the $Y_{3-x}Yb_xAl_5O_{12}$ $(0.00 \le x \le 0.09)$ ceramic pellets, as previously mentioned. Clearly, the YAG and Yb-substituted YAG ceramics show a linear tendency in the log-log graphs, regardless of the substitution ratios and bias voltages. All the graphs illustrate that the conductivity obeys a power exponent law, as follows [20, 21]:

$$\sigma(\omega, V, x) = \sigma_0(V, x)\omega^n$$

where $\sigma_0(V, x)$ denotes the proportionality pre-coefficient of AC conductivity as a function of both the bias voltage and substitution ratio, and $n(V, x)$ is the power exponent that varies with both the bias voltage and substitutional level with reference to the YAG. For this reason, the power exponent can be easily calculated from the slope of the plots of $log\sigma_{AC}$ versus $log\omega$ for the YAG and $Y_{3-x}Yb_xAl_5O_{12}$ $(0.00 \le x \le 0.09)$ ceramics. The power exponent is quantitatively dimensionless and approximately equal to unity.

For the unity value, the hopping mechanism is influential, otherwise there is always band conduction regardless of the applied constant electric field. As can be seen from Fig. 6, when all conductivities are carefully examined, it is clear that there is no fluctuation at any frequency and bias voltage and for any substitution ratios (including $x = 0.00$). However, any effect on the conductivity of the bias voltage was not measured, while a small deviation on the conductivity at lower frequencies is observed with a variation of the parameter.

As can be clearly seen from Fig. 6, an improved power exponent variation of the AC conductivity shows a steady trend for the YAG. However, for $Y_{3-x}Yb_xAl_5O_{12}$ ceramics, for $x = 0.01$, the AC conductivity decreased at all frequency ranges and bias voltages while it increased for other substitution levels, particularly at medium and high frequencies, as shown in Fig. 7, from the plots depicted at low (10.0 Hz),

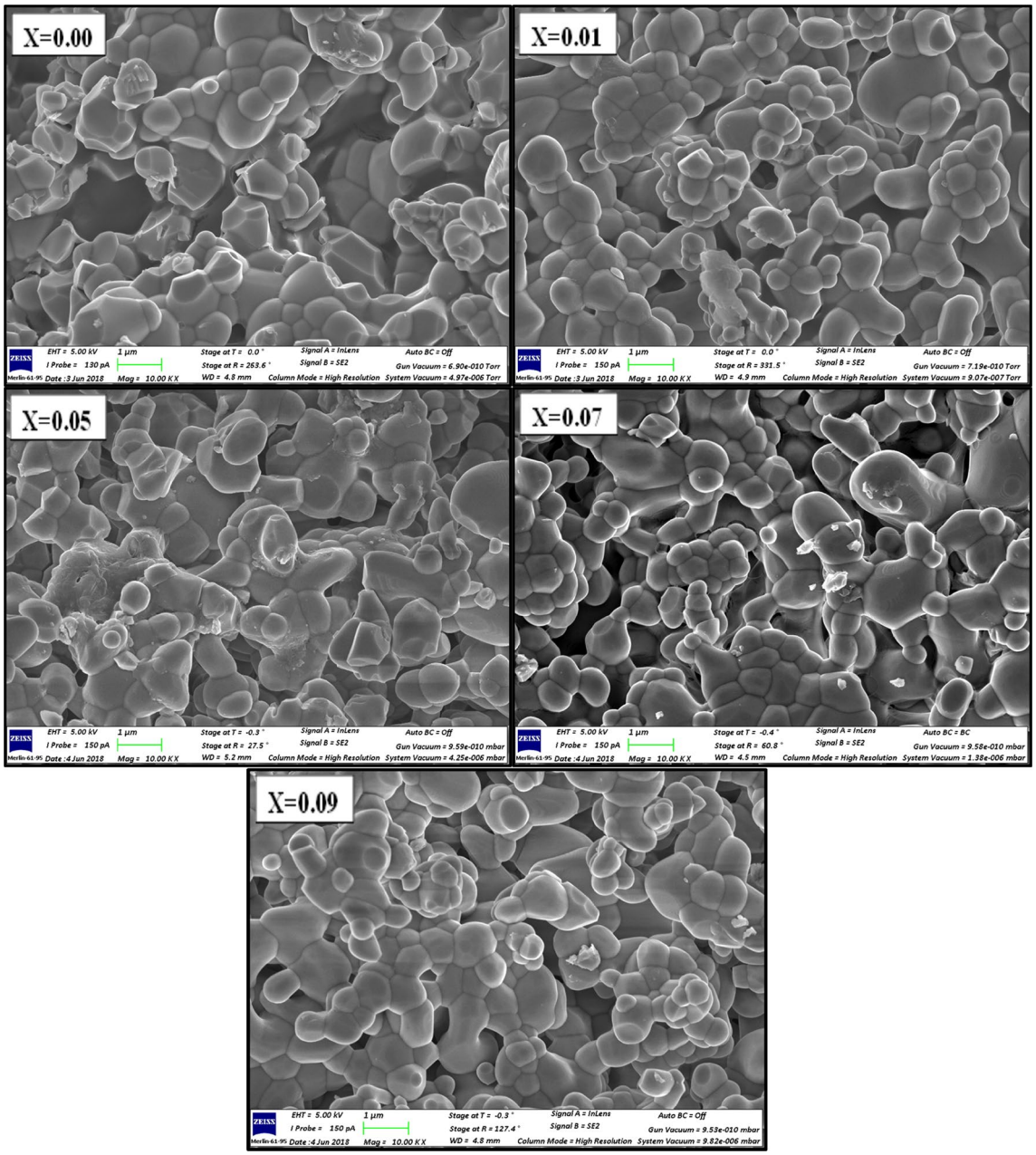

Fig. 3 SEM images of $Y_{3-x}Yb_xAl_5O_{12}$ ($0.00 \le x \le 0.09$)

medium (10.0 kHz), and high (10.0 MHz) frequencies. It should also be emphasized that the conductivity taken at the lowest frequency, 10 Hz, demonstrates the DC conductivity contribution originating from band conduction while both the medium and high frequency conductivity provides a contribution from the hopping mechanism, as described earlier. Hence, the band conduction mechanism is more dominant for Yb substitutional levels. It is obvious to note that some lower frequency conductivities up to 300 Hz provide a significant insight with an influence of Yb^{3+} ions over the substitutional level.

The externally-applied constant electric field has no effect on the conductivity for all ranges of frequencies and Yb^{3+} ion substitutions, except the conductivity at 10.0 Hz and for $x = 0.05$ for bias voltages of − 10.0 V and − 8.0 V. Therefore, this trend shows the ohmic type of the conductivity owing to its non-variation under the constant electric field applied across the sampling pellets studied here.

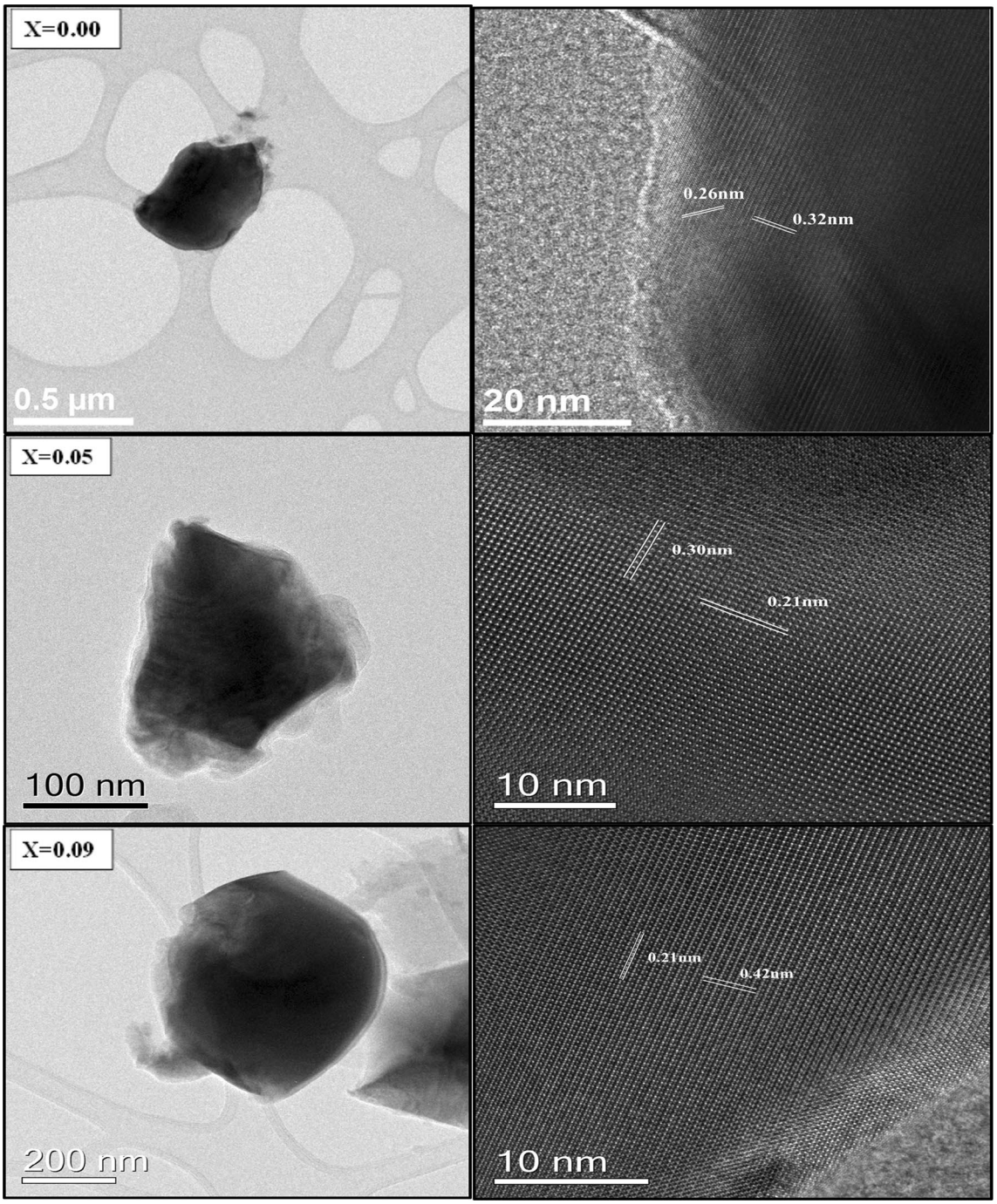

Fig. 4 TEM and HR-TEM images of $Y_{3-x}Yb_xAl_5O_{12}$ (x = 0.00, 0.05 and 0.09)

It can be seen from Fig. 7 that the conductivity almost increases with the level of frequency, i.e., $\sigma = 24$ pS/cm for 10 Hz; $\sigma = 20$ nS/cm for 10.0 kHz; and $\sigma = 35$ μS/cm for 10.0 MHz.

The above phenomenal attitudes may be owing to some ohmic type conduction contribution to the conductivity. The rest implies that the conduction phenomenon is AC conduction owing to the hopping of charge carriers across the sites. In general, the conductivity of non-doped YAG

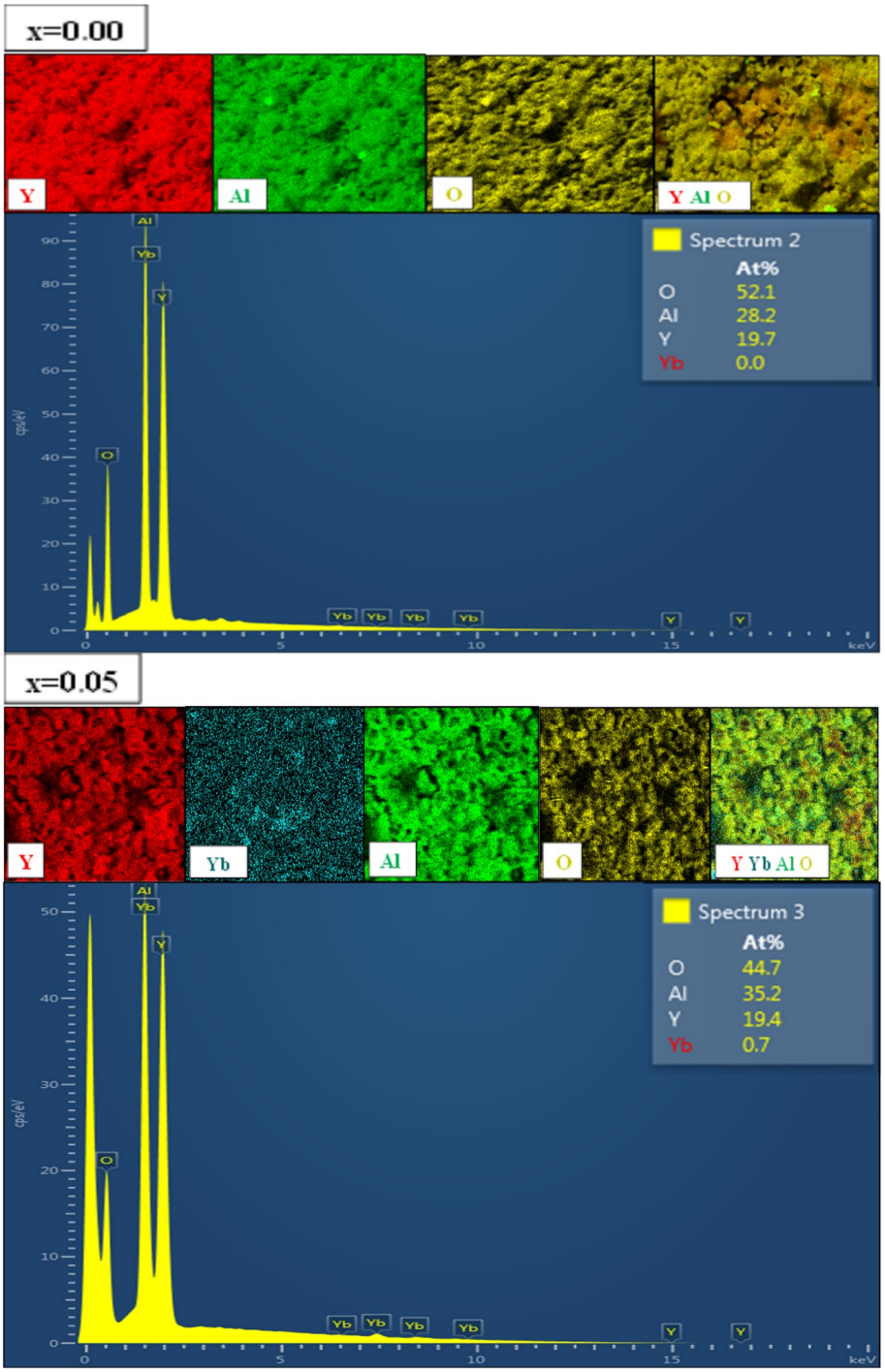

Fig. 5 EDX and elemental mapping spectra of $Y_{3-x}Yb_xAl_5O_{12}$ (x = 0.00 and 0.05)

decreases quickly with $x = 0.01$ and increases with any other level of substitutional ytterbium ions, while the frequency is strongly power law-dependent though independent of bias voltages. It is known that these types of tendencies could be allowed for general dielectric behavior and could also be interpreted on the basis that the hopping conduction increases with the elevation of frequencies. Hence, it is supported by the hopping electron conduction between the octahedral and tetrahedral symmetries of aluminum, although some charge carriers are released from different trapping centers. In the literature, there is an absence of information on the dielectric properties of YAG:xYb^{3+} ceramics, apart from the optical properties [22].

3.3.2 Nyquist plotting

For a given frequency, the real $Z'(\omega)$ and imaginary $Z''(\omega)$ parts of the complex impedance of YAG ceramics can be

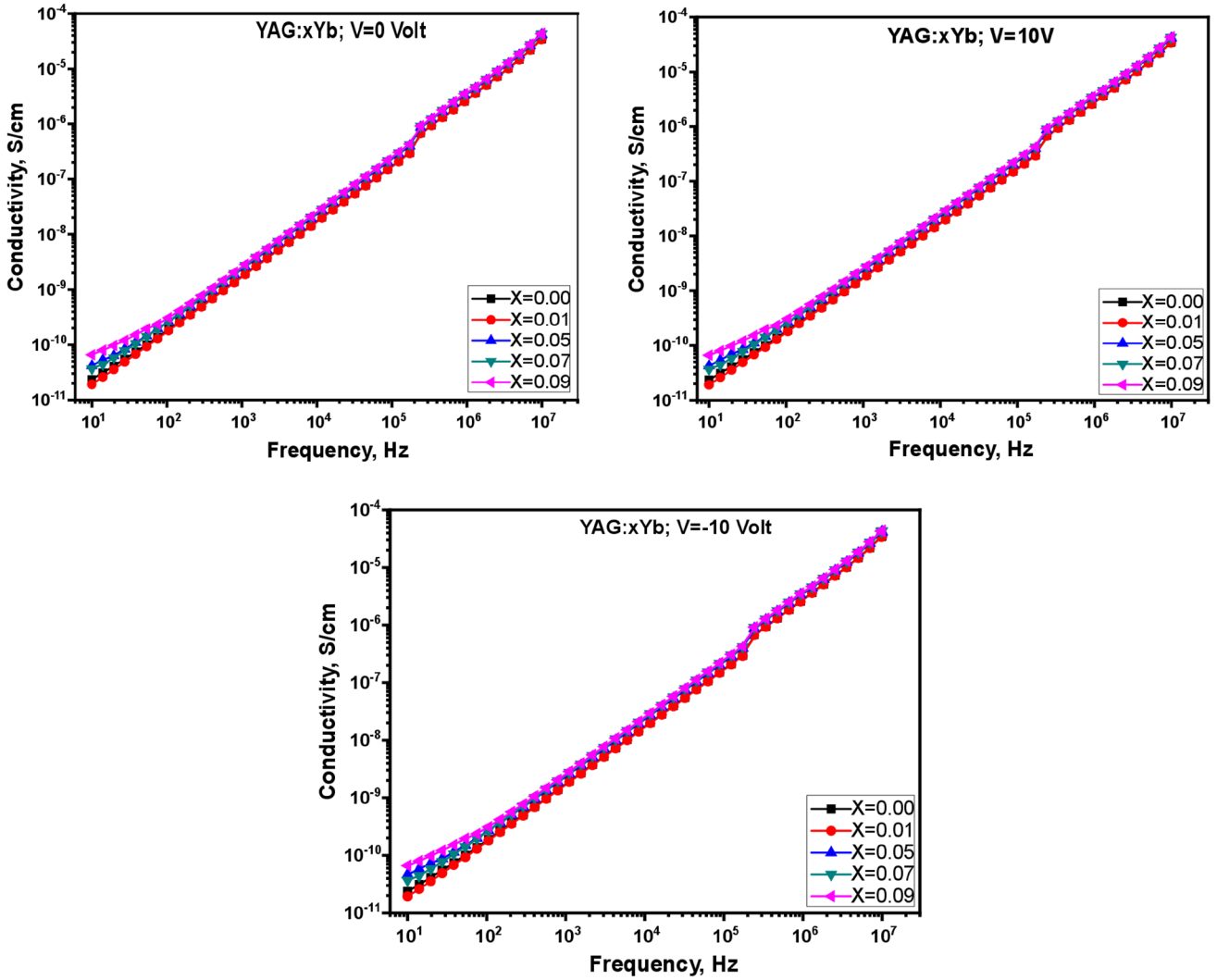

Fig. 6 *ac* conductivity plots of $Y_{3-x}Yb_xAl_5O_{12}$ $(0.00 \le x \le 0.09)$ ceramics as a function of frequency for various bias voltages. (Note that since the bias voltage dependence of the dielectric parameters is found to be insignificant, other graphs based on bias-voltages of −8 V, −6 V, −4 V −2 V, 2 V, 4 V, 6 V and 8 V are not shown)

expressed as $Z^*(\omega) = Z'(\omega) + iZ''(\omega)$. This can be determined from the complex permittivity $\varepsilon^*(\omega) = \varepsilon'(\omega) - i\varepsilon''(\omega)$ from the following expression: $Z^* = 1/(i\omega C_0 \varepsilon^*)$, where C_0 is capacitance in free space. Thus, the complex impedance of YAG ceramics could be given by the equation

$$Z^* = \frac{1}{R_g^{-1} + iwC_g} + \frac{1}{R_{gb}^{-1} + iwC_{gb}} = Z' - iZ''.$$

In the case of any substituted YAG ceramics, the dielectric behavior is typically controlled by any volumetric ratio of grains to grain boundaries. At lower frequencies, the contribution of grain boundaries to conduction is more dominant than that of grains. Owing to a poorer conduction, the motion of charge carriers is reduced at the grain boundary; hence, grain boundaries are less conductive than grains. A similar behavior pattern was noticed for Yb^{3+} ion-substituted YAG ceramics because the resistance of the grain boundaries was found to be relatively larger than that of the bulky grains. This indicates that grain boundaries act as a barrier in the conduction mechanism. Yet, Yb^{3+} ion substitution reduces the resistance of grain boundaries, making it comparable to that of the grain boundaries of YAG ceramics [23].

As a characteristic evaluation, Nyquist plot is an essential tool to investigate the effect of the microstructures of YAG ceramics on the conduction mechanism. The analysis of Nyquist plots provides some significant parameters relevant

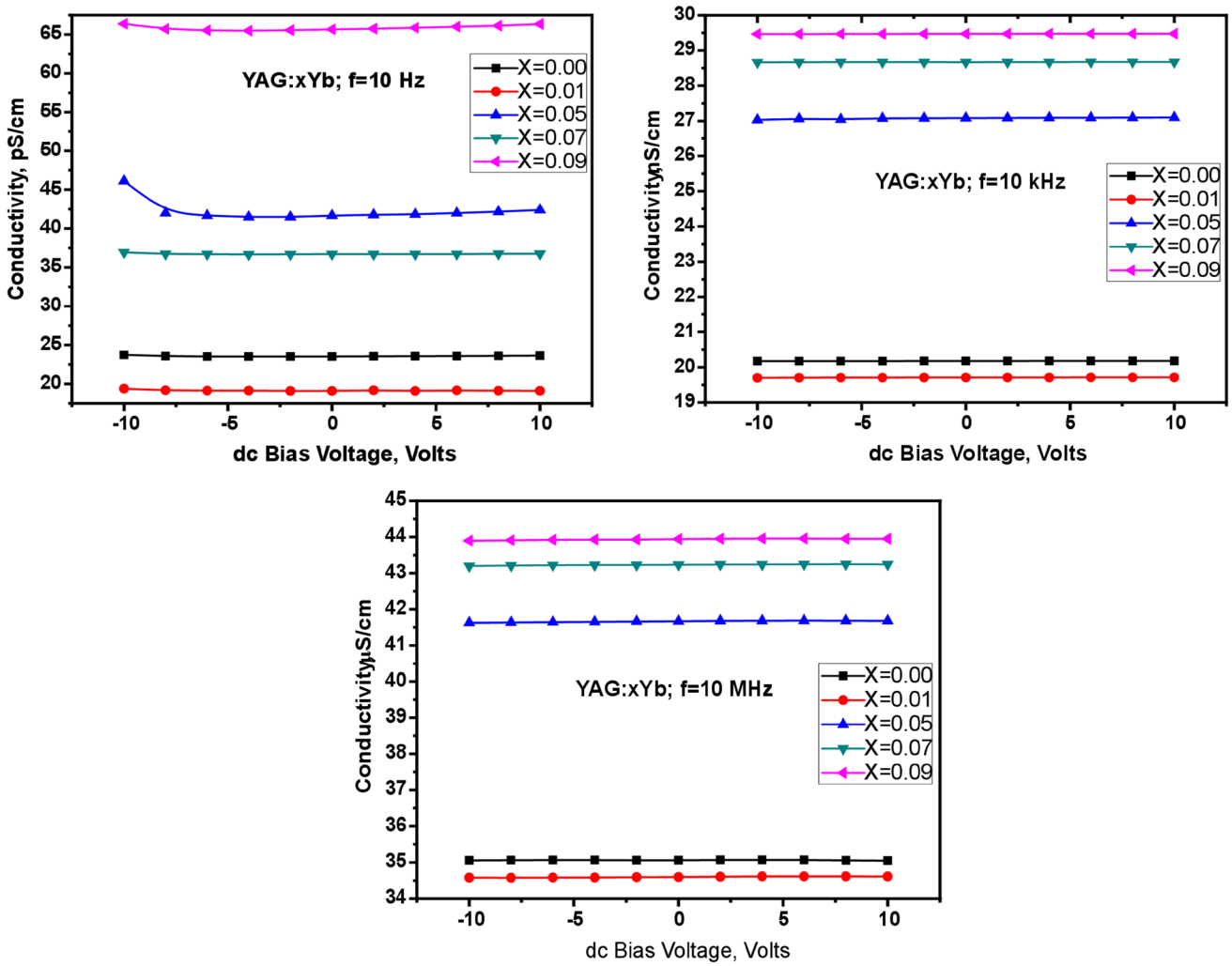

Fig. 7 *ac* Conductivity plots of $Y_{3-x}Yb_xAl_5O_{12}$ ($0.00 \le x \le 0.09$) ceramics as a function of dc bias voltage for various substitutions

to non-Debye relaxation approaches. Figure 8 shows that, first, there is no effect of magnitude and polarity of the bias voltage on the Nyquist plot and, secondly, with the elevation of frequencies between 10 Hz and 10 MHz, the variation of reactance against resistance for $x = 0.01$ seems to be quite high when compared with other substitutions as well as pure YAG ceramics. Thirdly, for the same range of frequencies (10 Hz–10 MHz), the magnitude of reactance varies up to 6 GΩ for $x = 0.01$, while that of the resistance reaches 46 GΩ for the same substitutions, but for a bias voltage of 10.0 V.

3.3.3 Dielectric constant

The dielectric measurements of both YAG and $Y_{3-x}Yb_xAl_5O_{12}$ ($0.00 \le x \le 0.09$) ceramics were carried out at a frequency between 10.0 Hz and 10.0 MHz and at a voltage between − 10.0 and 10.0 V, with an interval of ΔV = 2.0 V. An investigation of the dielectric parameters, such as dielectric constant, dielectric loss, and dielectric tangential loss factor, provides useful information on the transport of electric charge carriers in terms of understanding the conduction mechanism of $Y_{3-x}Yb_xAl_5O_{12}$ ($0.00 \le x \le 0.09$) ceramics. As shown in Fig. 9, the dielectric constant exponentially decreases with increasing frequency up to 173.0 kHz before bouncing between the values of 4 and 6, then exponentially increasing with increasing frequencies starting at 242.0 kHz for both YAG and $Y_{3-x}Yb_xAl_5O_{12}$ ceramics for $x = 0.01$. For other substitutional YAG samples, the tendencies in the second region seem quite different. It was observed that the dielectric constant strongly depends on the substitution rates in YAG ceramics. In this case, after bouncing between a value from 5.5 to 7.9 ($x = 0.09$), it remained almost constant along a frequency of 950 kHz, before suddenly dropping to 7.5 by

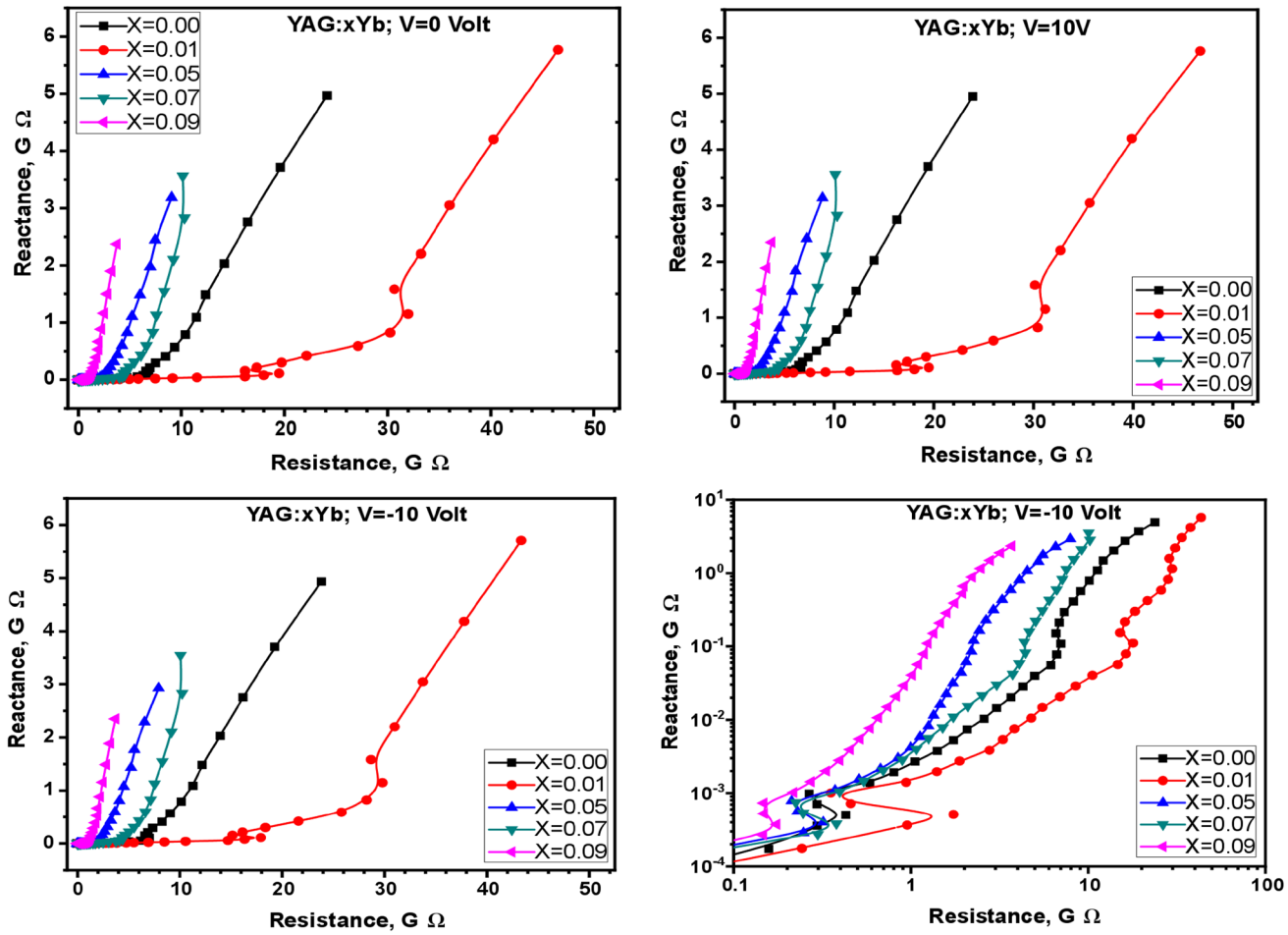

Fig. 8 Nyquist plots of $Y_{3-x}Yb_xAl_5O_{12}$ ($0.00 \le x \le 0.09$) ceramics for various substitutions and bias voltages. The last graph represents the log–log Nyquist plot to see that the low frequency effect is even clearer

1.35 MHz ($x = 0.09$), then exponentially increasing with increasing frequencies. Therefore, such a change in the dielectric constant can be easily modified by the substitution level of Yb^{3+} ions in YAG ceramics relative to a particular frequency domain. It is observed that the dielectric constant has a value between 4 and 11, depending on both the frequency and the substitution level. However, no significant change was recorded for a variation in the magnitude and polarity of the externally-applied DC bias voltages.

In addition, the dielectric constant reduced by a multiple exponential trend, unlike by a power exponent or simple exponential trend. In general, the bias voltage does not have an effect on the dielectric constant, while the ytterbium substitution causes a significant increase in the dielectric constant.

The dielectric constant as a function of frequency for the whole substitution level shows some different properties. This is attributed to the electrical conduction owing to both the electron and polar jumping mechanisms. Because of the complexity of various $Y_{3-x}Yb_xAl_5O_{12}$ ($0.00 \le x \le 0.09$) ceramics, as already mentioned for two types of symmetry, the dielectric constant depends on how quickly the polarization level communicates with the stimulus of an externally-applied electric field oscillation. The higher the frequency, the lower the polarization orientation, because the alignment of the dipole moments requires a longer interval of response time compared to the orientation of the electronic and ionic polarizations.

This results in a reduction in the dielectric constant, and the exponential decay rate varies for all samples depending on both the frequency and the substitution rate of the Yb^{3+} ions. The frequency dependence of the dielectric constant describes the presence of the

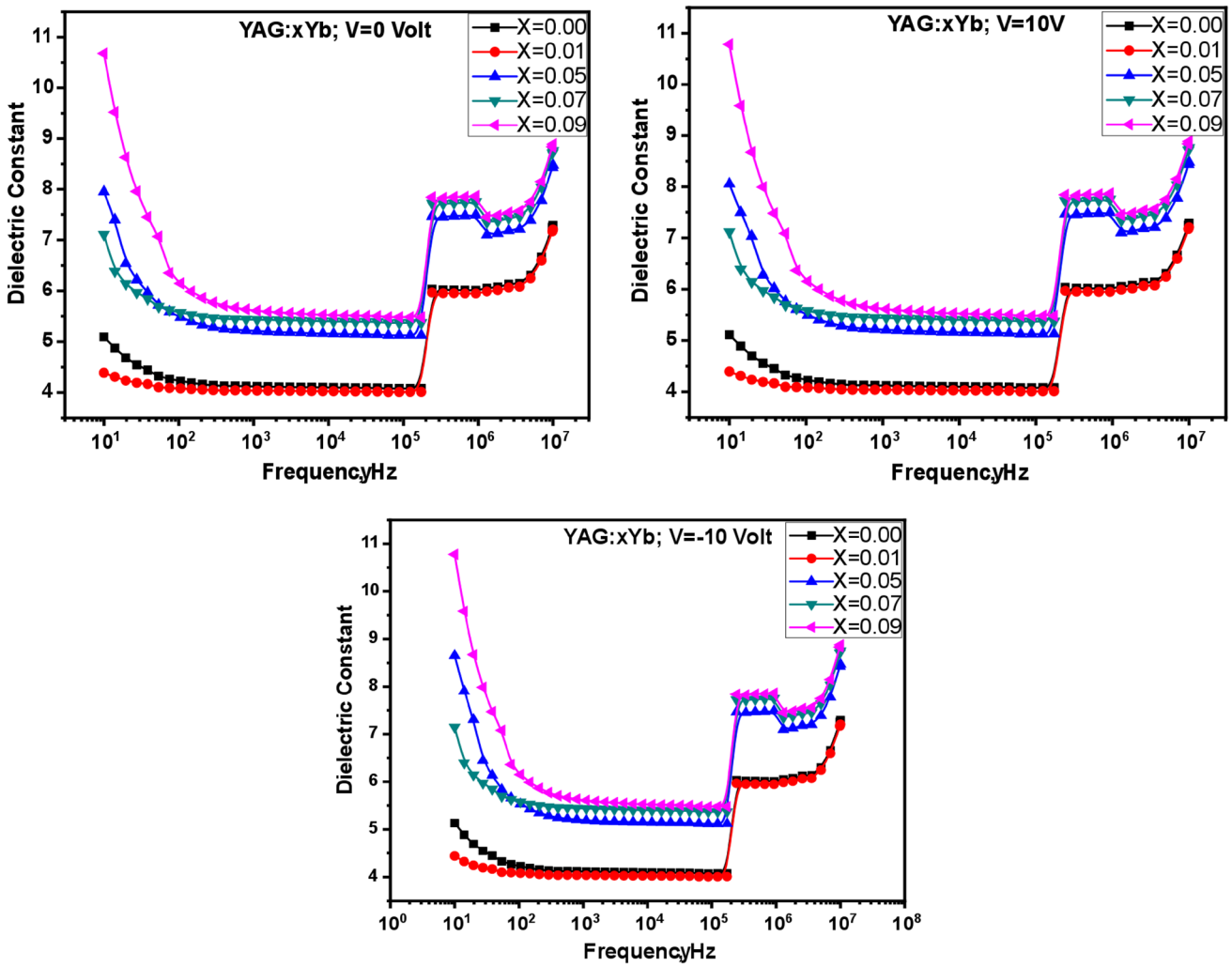

Fig. 9 Dielectric constant plots of $Y_{3-x}Yb_xAl_5O_{12}$ ($0.00 \le x \le 0.09$) ceramics as a function of frequency for various bias voltages

electrode interface polarization processes, which are usually seen at lower frequencies. Incremental substitution dependence may possibly be attributed to molecular orientation and rearrangement [24, 25]. For this reason, the dielectric constant of $Y_{3-x}Yb_xAl_5O_{12}$ ($0.00 \le x \le 0.09$) ceramics increases with the substitution rate owing to the improvement in the boundaries between some lanthanide ion substitutions in YAG as the dopant concentration varies.

3.3.4 Dielectric loss

In general, the dielectric loss for both YAG and $Y_{3-x}Yb_xAl_5O_{12}$ ($0.00 \le x \le 0.09$) ceramics showed a power law trend, that is, a nearly linear curve in the log–log graphs. The frequency dependency of the dielectric loss shows an almost linear decrease up to the frequency of 65 kHz. Then, the various fluctuations in the higher frequency region depend on the substitutional level and type, and even frequency region. However, there is no significant effect on the dielectric loss of the magnitude and polarity of bias voltages.

This linearity in the 10–65,000 Hz frequency range of the log–log graphs related to the power law of the base of n is defined by

$$\varepsilon''(\omega;x) = \varepsilon''(0;x)\omega^n$$

where ω is the angular frequency and $\varepsilon''(0;x)$ is the pre-coefficient dielectric loss that is dependent on substitutional ratios, as shown in Fig. 10. n is the power exponent

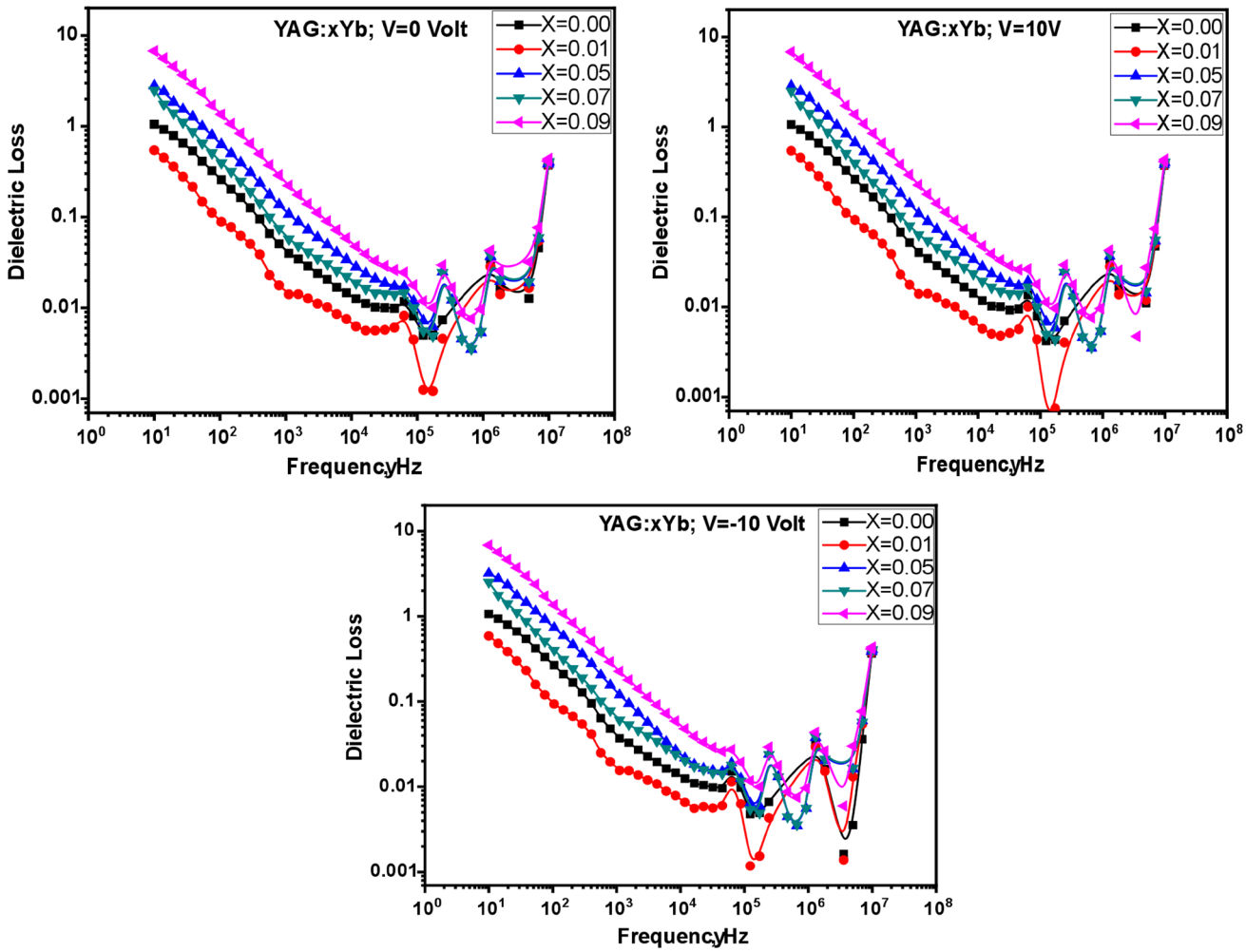

Fig. 10 Dielectric loss plots of $Y_{3-x}Yb_xAl_5O_{12}$ ($0.00 \le x \le 0.09$) ceramics as a function of frequency for various bias voltages

associated with the substitution of Yb^{3+} ions in YAG and also with YAG itself. For this reason, it can be assumed that the dielectric loss mechanism depends on the nature of the reorganization owing to the structural diffusion of the elemental substitutions. It is also clear that the capacitive response exhibits a higher dielectric loss dependence when compared to the rearrangement of the Yb^{3+} ion substitution in YAG. In the log–log graph, this linearity corresponds to the DC conductivity (σ_{DC}) expressed as

$$\varepsilon''_{dc} = \sigma_{dc}(\omega C_o)$$

where C_o is the vacuum capacitance. The dielectric loss eventually reaches a minimum level, with some fluctuations at the end of a higher frequency and is usually shifted to the higher frequency side depending on the substitution rate of the Yb^{3+} ions in the YAG. Owing to the charge transfer between the symmetries of the Al ions, there is a limited drift motion of charges in the direction of the externally-applied electric field establishing the polarization. Therefore, the polarization degree decreases with increasing frequency as the electronic transition between the symmetries of the Al ions delays the following electric field.

3.3.5 Dielectric modulus

The dielectric modulus can be divided into both real and imaginary components of the complex dielectric data related to the dielectric constant ε' and dielectric loss ε'', and can be expressed with an equation [26]:

$$M^* = \frac{1}{\varepsilon^*} = M' + iM'' = \frac{\varepsilon' + i\varepsilon''}{\varepsilon'^2 + \varepsilon''^2}$$

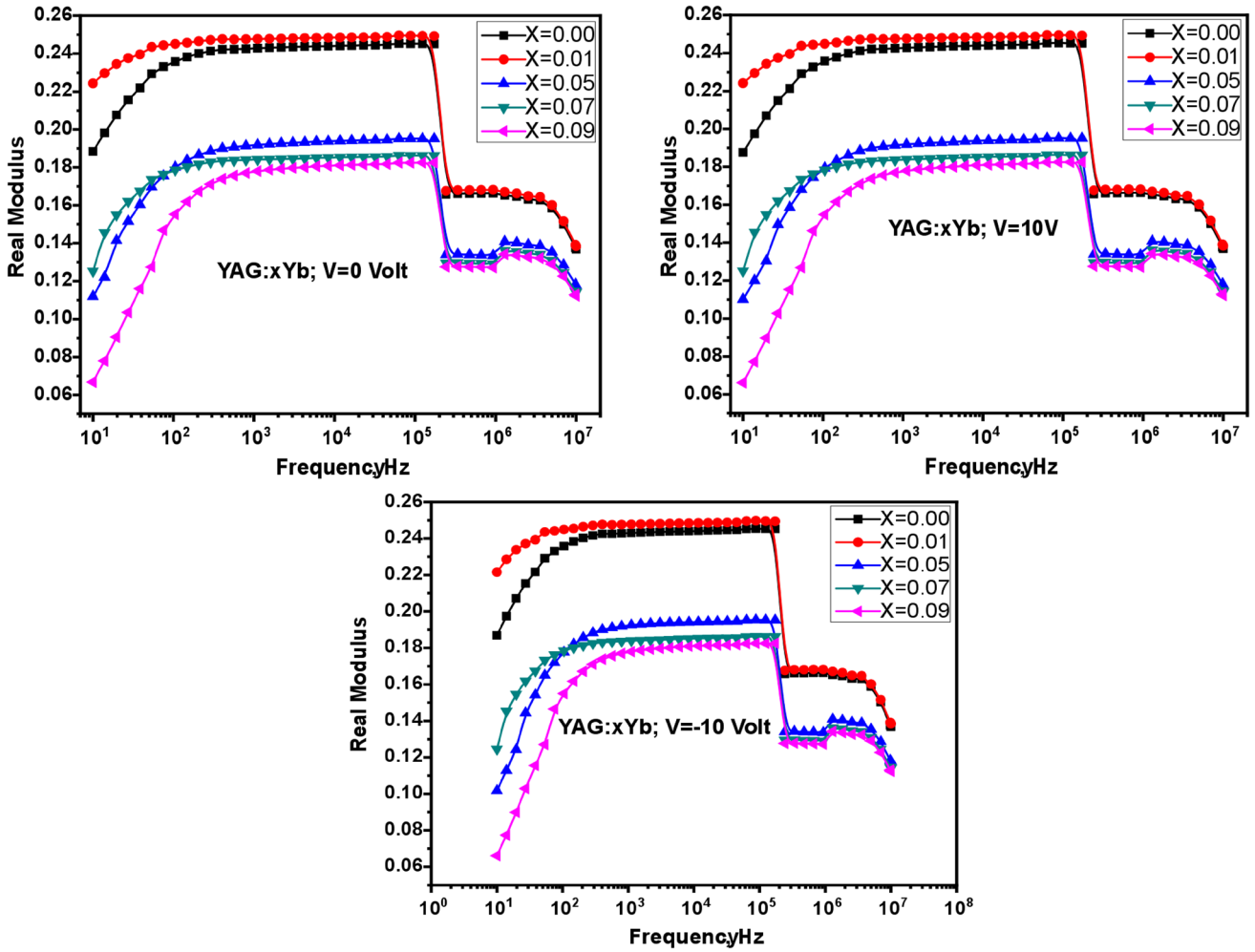

Fig. 11 Real modulus plots of $Y_{3-x}Yb_xAl_5O_{12}$ ($0.00 \le x \le 0.09$) ceramics as a function of frequency for various bias voltages

where M' and M'' are the real and complex components of the dielectric modulus, respectively.

The real modulus measurement of $Y_{3-x}Yb_xAl_5O_{12}$ ceramics as a function of the frequency for various bias voltages is summarized for a variety of Yb^{3+} ion substitutions in Fig. 11. It is important to emphasize that the real modulus increases with increasing frequency before reaching a saturation level along a certain frequency of 165 kHz. It is observed that the real modulus has a similar trend as in the case of the mirror image curves of the dielectric constant. Hence, both results can be interpreted in a similar manner.

In Fig. 12, the imaginary modulus is studied as a function of the frequency up to 10.0 MHz of both YAG and Yb^{3+}-substituted YAG extensively for bias voltages ranging from − 10 to 10 V with an interval of 2 V. For both the YAG and Yb^{3+}-substituted YAG ceramics, the imaginary modulus first decreases rapidly to a frequency of 100 kHz, then continues to decrease slowly until the frequency reached 2.4 MHz, after this it increases by a certain value.

3.3.6 Dielectric tangent loss

For the tangent loss analysis, it is clear to see from Fig. 13 that the magnitude of the tangential loss at the lower frequencies is strongly dependent on the substitution but independent of the bias voltages. Over a medium frequency range of 1.0 kHz, the tangential loss is minimized and at higher frequencies, just below 10.0 MHz, it begins

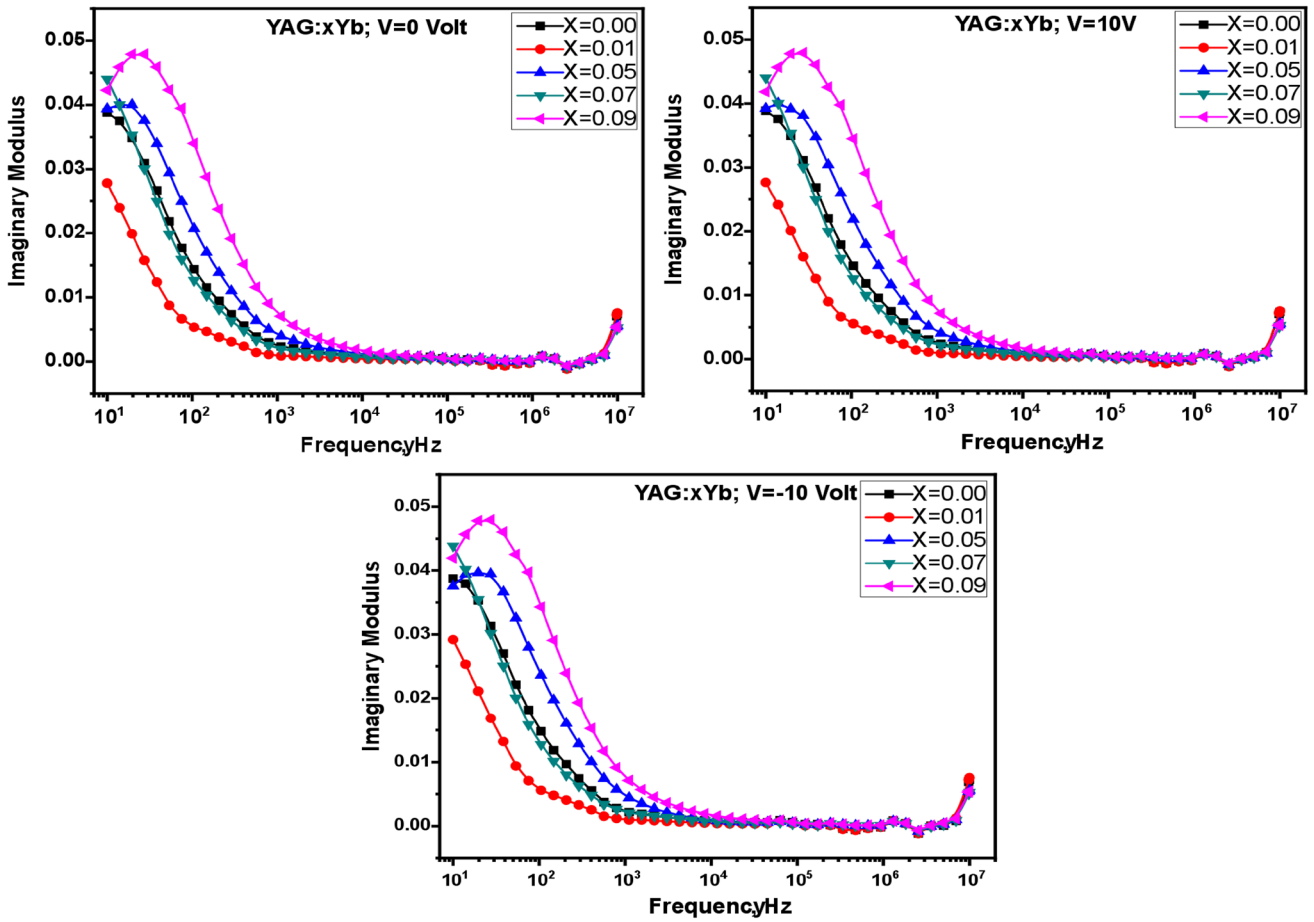

Fig. 12 Imaginary modulus plots of $Y_{3-x}Yb_xAl_5O_{12}$ ($0.00 \le x \le 0.09$) ceramics as a function of frequency for various bias voltages

to increase for all. Hence, the decline in both the dielectric constant and lossy tangent with the frequency is normal behavior within the octahedral and tetrahedral symmetries of the aluminum ions of YAG and can be attributed to charge polarization. The rapid reduction of both the dielectric constant and the lossy tangent with respect to frequency can normally be attributed to the structural symmetry of the aluminum ions in the YAG and, thus, to the charge polarization. Some rapid reduction in the tangential loss, similar to the dielectric constant, occurs owing to the frequency of the electron exchange between the structural symmetry sites of the aluminum atoms in YAG, which does not originate from any externally-applied electric field.

4 Conclusion

$Y_{3-x}Yb_xAl_5O_{12}$ ($0.00 \le x \le 0.09$) ceramics were prepared via a solid-state reaction. X-ray powder pattern and HRTEM confirmed the YAG cubic structure. The electrical and dielectric properties of YAG ceramics up to a frequency of 10.0 MHz were examined; it was observed that the ytterbium dependency is better understood by the parametric variations such as conductivity, dielectric constant, and loss mechanisms. This tendency can be attributed to various lattice modifications such as 3d-Al ions and 4f-Yb ions in the structural symmetries in YAG:xYb^{3+} ceramics.

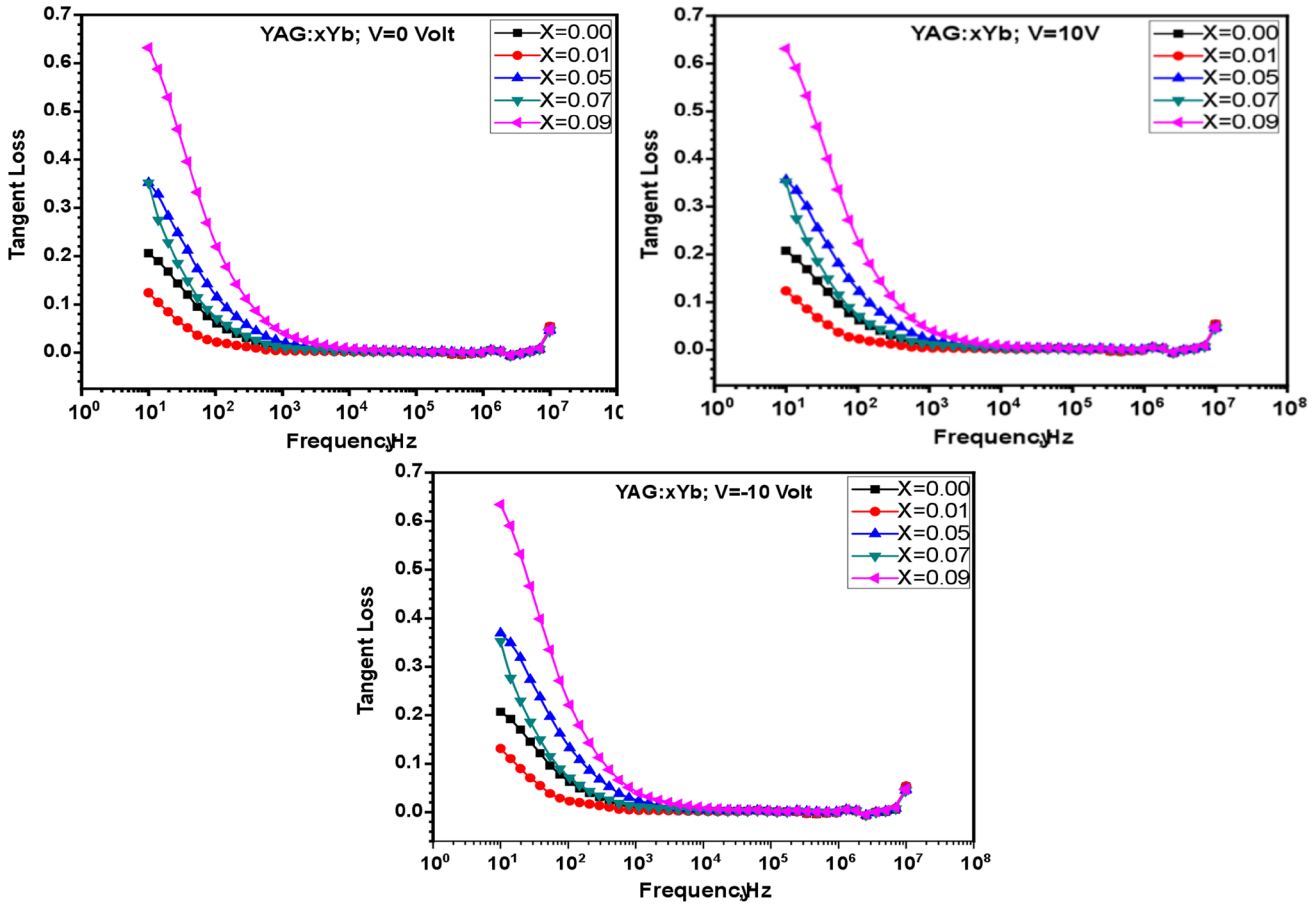

Fig. 13 Semilog tangential loss plots of $Y_{3-x}Yb_xAl_5O_{12}$ ($0.00 \le x \le 0.09$) ceramics as a function of frequency for various bias voltages

References

1. S.H. Yoon, D.W. Kim, S.Y. Cho, K.S. Hong, J. Eur. Ceram. Soc. **26**, 2051–2054 (2006)
2. A. Sunny, V. Viswanath, K.P. Surendran, M.T. Sebastian, Ceram. Int. **40**, 4311–4317 (2014)
3. T. Tsunooka, M. Androu, Y. Higashida, H. Sugiura, H. Ohsato, J. Eur. Ceram. Soc. **23**, 2573–2578 (2003)
4. S. Thomas, M.T. Sebastian, J. Am. Ceram. Soc. **92**, 2975–2981 (2009)
5. Y. Slimani, E. Hannachi, A. Hamrita, M.K. Salem, F. Ben Azzouz, A. Manikandan, M.K. Salem, Ceram. Int. **44**, 19950–19957 (2018)
6. R. Tummala, M. Kosec, W.K. Jones, D. Belavic, *Electronic Packaging for High Reliability, Low Cost Electronics*, vol. 57 (Kluwer Academic Publishers, Dordrecht, 1999), pp. 65–75
7. K. Maexa, M.R. Baklanov, D. Shamiryan, F. Iacopi, S.H. Brongersma, Z.S. Yanovitskaya, J. Appl. Phys. **93**, 8793–8841 (2003)
8. G. Seeta, R. Raju, H. Chae, J. Jin, Y. Park, J.W. Chung, B.K. Moon, J.H. Jeong, S.M. Son, J.H. Kim, J. Optoelectron. Adv. Mater. **12**, 1273–1278 (2010)
9. Y. Hakuta, T. Haganuma, K. Sue, T. Adschiri, K. Arai, Mater. Res. Bull. **38**, 1257–1265 (2003)
10. H.M.H. Fadlalla, C.C. Tang, E.M. Elssfah, F. Shi, Mater. Chem. Phys. **109**, 436–439 (2008)
11. K.V. Benthem, C. Els¨asser, R.H. French, J. Appl. Phys. **90**, 6156–6164 (2001)
12. Y. Slimani, A. Baykal, N. Md. Amir, H. Tashkandi, S. Güngüneş, H.S. Guner, F. El Sayed, T.A. Aldakheel, A. Saleh, Manikandan, Ceram. Int. **44**, 15995–16004 (2018)
13. A.G. Abraham, A. Manikandan, E. Manikandan, S. Vadivel, S.K. Jaganathan, A. Baykal, P.Sri Renganathan, J. Magn. Magn. Mater. **452**, 380–388 (2018)
14. J. Park, K.H. Kim, J. Yoon, M. Song, T. Kim, H. Hur, J. Eur. Ceram. Soc. **29**, 1735–1741 (2009)
15. S. Geller, Zeitschrift Für Kristallographie-Cryst. Mater. **125**, 1–47 (1967)
16. P. Nørby, K.M.Ø Jensen, N. Lock, M. Christensen, B. Iversen, Cryst. Growth **16**, 2646–2652 (2016)
17. E. Hema, A. Manikandan, M. Gayathri, M. Durka, S. Arul Antony, B.R. Venkatraman, J. Nanosci. Nanotechnol. **16**, 5929–5943 (2016)
18. S. Asiri, S. Güner, A. Demir, A. Yildiz, A. Manikandan, A. BaykalEmail, J. Inorg. Organomet. Polym. Mater. **28**, 1065–1071 (2018)
19. Y. Bakış, I.A. Auwal, B. Ünal, A. Baykal, Ceram. Int. **42**, 11780–11795 (2016)
20. A. Zafar, A. Rahman, S. Shahzada, S. Anwar, M. Khan, A. Nisar, M. Ahmad, S. Karim, J. Alloy. Compd. **727**, 683–690 (2017)
21. B. Want, B.H. Bhat, B.Z. Ahmad, J. Alloy. Compd. **627**, 78–84 (2015)
22. X. Xu, Z. Zhao, P. Song, G. Zhou, J. Xu, P. Deng, J. Opt. Soc. Am. B **21**, 543–547 (2004)

23. C. Li, H. Zuo, M. Zhang, J. Han, S. Meng, Trans. Nonferrous Metals Soc. China **17**(1), 148–153 (2007)
24. H. Sözeri, F. Genç, B. Unal, A. Baykal, B. Aktas, J. Alloy. Compd. **660**, 324 (2016)
25. S. Minemoto, H. Nanjo, H. Tanji, T. Suzuki, H. Sakai, J. Chem. Phys. **118**, 4052 (2003)
26. Md. Amir, B. Unal, M. Geleri, H. Güngüneş, E. Sagar, S.E. Shirsath, A. Baykal, Superlattices Microstruct. **88**, 450 (2015)